Practical Determination of Passive Intermodulation From Modulated Signals in Satellite Applications

Davide Smacchia, Mónica Martínez-Mendoza, Carlos Alcaide, Pablo Soto, *Member, IEEE,* Vicente E. Boria, *Fellow, IEEE,* and David Raboso

***Abstract*—Passive Intermodulation (PIM) measurements are typically conducted with a simplified test scenario composed by two radiofrequency (RF) carrier tones operating in continuous wave (CW). However, satellite payloads tend to operate with a more complex scheme, where modulated signals are present at each transmission channel. This paper aims at linking both PIM scenarios. A novel procedure is developed to obtain, from measured data obtained using two CW input tones, the spectral distribution and amplitude of a PIM contribution originated after exciting a non-linear device with modulated signals. The technique determines the spectral distribution of the PIM term of interest from the spectrum of the input signals, and evaluates its amplitude from a recently formulated PIM power conservation rule. Moreover, an extensive PIM test campaign providing novel and valuable experimental data for the topic of PIM under modulated signal excitation has been carried out. The results obtained for a wide range of test scenarios exhibit a good agreement with theoretical predictions, thus providing a practical validation of the proposed technique.**

***Index Terms*—Distortion measurement, intermodulation distortion, modulation, passive circuits, satellite communications.**

I. Introduction

PASSIVE Intermodulation (PIM) interference has been faced since the 70s of the 20th century, when several space programs such as FLTSATCOM, LES6, MARISAR, among others, suffered PIM issues during their testing phases [1], [2]. For those cases, PIM caused a redesign of the satellite architecture, with consequent schedule slippage and added cost to the missions.

Nowadays, despite some heritage and lessons learnt from the past, PIM still represents a major threat for the space industry. In fact, common satellite payloads have a high number of transmission channels in the downlink to improve flexibility and bandwidth usage, leading to a multicarrier scenario which fosters intermodulation issues [3]–[7].

Manuscript received September XX, 2024; revised YY XX, 2024. This work was supported in part by the Ministerio de Ciencia e Innovación, MCIN/AEI/10.13039/501100011033, Spanish Government, under Research and Development Grants PID2022-136590OB-C41 and TED2021-129196B-C41, and in part by the European Space Agency (ESA) through several Research and Development activities. *(Corresponding author: Pablo Soto.)*

D. Smacchia is with ESA-VSC European High Power RF Space Laboratory, Valencia, E-46022, Spain (e-mail: davide.smacchia@val-space.com).

M. Martínez-Mendoza, C. Alcaide, P. Soto and V. E. Boria are with iTEAM, Universitat Politècnica de València, Valencia, E-46022, Spain (e-mail: momarmen@iteam.upv.es; calcaide@iteam.upv.es; pabsopac@dcom.upv.es; vboria@dcom.upv.es).

D. Raboso is with European Space Research and Technology Centre of the European Space Agency (ESTEC-ESA), Noordwijk, 2200 AG, The Netherlands (e-mail: david.raboso@esa.int).

Color versions of one or more figures in this paper are available at https://doi.org/10.1109/TMTT.2025.XXXXXXX.

The situation is even worse for modern High Throughput Satellites (HTS) payloads operating at higher frequency bands [8], [9]. In fact, the compact sizes of these payloads (due to the higher operational frequency), combined with the high data rates (throughput), leads to adopt architectures implying elevated surface current densities for the transmitted signals. This is indeed a typical ignition factor of passive intermodulation [10]–[13], which may cause that harmful PIM terms generated in the downlink may fall in the reception band and interfere with the weak signals to be received, thus jeopardizing the uplink performance.

Traditional PIM models and measurement standards consider a simplified scenario composed by two continuous wave (CW) tones [14], [15]. Such a scenario, however, is far from the real operation of payload satellites, where the downlink is typically composed of a large number of modulated signals, which are combined using a frequency division multiplexing (FDM) scheme with equi-spaced channels [16].

The finding of a link between the aforementioned typical reduced scenario, considered for standard PIM measurements, and the actual operation case with modulated signals, is therefore of great practical interest. The understanding of this relationship could be of help to estimate the PIM performance of the key hardware of a system, from measured data obtained in the usual standard test scenario [15], without requiring specific PIM measurements in more complex schemes involving modulated signals. In order to establish such a link, the PIM power conservation rule recently proposed in [17] can be useful, since it is able to account for the power spreading as the PIM spectrum enlarges. Note that this heuristic law is applicable to PIM, but it has not been observed in the case of active intermodulation (AIM) so far.

At this point, it is important to mention that the causes and principles of PIM can differ from those governing active intermodulation (AIM) [18]–[20]. In fact, the PIM power level does not seem to follow the general rule of N dB growth for each dB of input power increase for an N-th order term [21]. Roughly constant slope factors SF in the range of 1.6-3 dB/dB of input power for third order PIM terms, and about 2.3-3 dB/dB for fifth order terms have been experimentally obtained for different practical applications [14], [22]–[24]. Therefore, the well-established results for AIM cannot be directly extrapolated to passive intermodulation. This fact, together with the challenging nature of PIM (primarily originated by slight imperfections in metal-to-metal contacts and workmanship [10], [11]), makes the development of reliable passive intermodulation predictions tools extremely difficult.

As a result, PIM characterization must rely on experimental verification.

This paper proposes a novel technique to estimate the spectrum of a PIM term originated from two channels with modulated signals. A theoretical model is presented to obtain the shape of the PIM spectrum from the spectral distribution of the two input modulated signals. The determination of the amplitude of the PIM term, however, requires experimental data from the device under test (DUT). For this reason, a novel link is introduced by using a recently proposed PIM power conservation rule [17]. Thanks to this link, the amplitude of the PIM term can de derived from measurements performed in the simplified standard scenario corresponding to two input CW tones [14], [15]. The analysis is focused on the 3rd order PIM term, the most critical one in satellite applications [14], [23], [24]. However, it can be easily extended for other PIM terms if required. An extensive Ku-band PIM test campaign involving both modulated and CW signals is performed, providing novel valuable experimental data. After verifying the application of the PIM power conservation rule to modulated signals and verify the effect of different modulation parameters, a range of diverse scenarios are considered. An excellent match between the theory and the real measurements is demonstrated, proving the validity of the proposed technique.

II. Theory

A. PIM Power Distribution

The standard scenario for PIM testing, which considers two input CW signals of the same power, has been deeply analyzed in practice [15], [25], [26]. However, the extension to more generic situations, such as the ones involving modulated or multicarrier signals, is a matter of research.

Some works in the technical literature analyze PIM under excitation schemes that go beyond the two equal-amplitude CW tone scenario. Most of them, however, do provide simulated data from the classic polynomial model [19]. This is the case in [27], [28], once the coefficients of the non-linear polynomial were adjusted to fit PIM measurements obtained from the standard two-carrier test.

A very complete set of experimental PIM data for a real multicarrier scenario was disclosed in [23]. The authors also observed that the power level of the PIM terms was affected by the presence of non-contributing carriers (i.e., carriers which are not theoretically related to the specific PIM term measured), although no explanation was given. An heuristic model fitting this set of measured data was reported more recently in [17], which states the PIM power corresponding to a specific non-linear order is related to the total amount of RF power at the input of the non-linear device in the form:

$$\begin{aligned} OP_{\text{PIM}}\,(\text{dBm}) &= OP_{\text{PIM},0}\,(\text{dBm}) \\ &\quad + SF \cdot (IP\,(\text{dBm}) - IP_0\,(\text{dBm})) \end{aligned} \tag{1}$$

where IP represents the overall input RF power, OP_{PIM} the output PIM power for a specific non-linear order, $OP_{\text{PIM},0}$ is the output PIM power for the non-linear order under consideration associated to an input RF reference power IP_0, and SF is the slope factor of such a non-linear order (i.e., the increase of output PIM power for an increase of 1 dB in the input RF power).

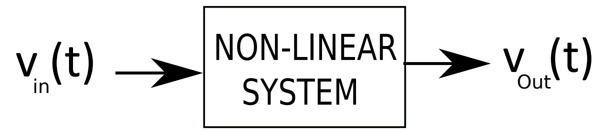

Fig. 1. Generic non-linear system, where the output signal $v_{\text{out}}(t)$ is a function of the input signal $v_{\text{in}}(t)$.

It is worth highlighting that the terms SF, $OP_{\text{PIM},0}$ and IP_0 in (1) can be experimentally obtained from a two-tone PIM test, thus enabling the characterization of a general PIM scenario by resorting only to the standard two-carrier testing normally used in practice. This was indeed the approach followed in [17] to justify the experimental results from [23], after distributing the overall output PIM power computed from (1) in the different third-order PIM terms originated from a multicarrier excitation by using:

$$OP_{\text{PIM},i}\,(\text{mW}) = OP_{\text{PIM}}\,(\text{mW}) \cdot \frac{AF_i^2}{\sum_j AF_j^2} \tag{2}$$

being $OP_{\text{PIM},i}$ the power of an specific i-th PIM term, whereas AF_k denotes the amplitude factor of the k-th PIM term of the order under consideration [17].

A similar approach is followed in this work for generic modulated signals. For an excitation composed of multiple CW carriers, the PIM terms are also pure CW tones. For modulated signal stimulus, however, the power of the resulting PIM contributions spreads out along the frequency axis depending on the spectral shape of the input modulated signals. This results in a lower PIM power spectral density when compared to the CW case with the same overall input power.

The PIM power conservation rule is a heuristic principle proposed for the first time in [17], where it provided excellent agreement with measured data from diverse multicarrier scenarios [23]. However, a further validation is recommended for other applications. In Section III-A, this heuristic rule has also been verified for the case of input modulated signals.

B. Model for PIM Originated From Modulated Signals

For the sake of simplicity, the following analysis is restricted to two generic signals $v_{\text{in1}}(t)$ and $v_{\text{in2}}(t)$ at the input of the non-linear system (see Fig. 1):

$$v_{\text{in}}(t) = v_{\text{in1}}(t) + v_{\text{in2}}(t) \tag{3}$$

although the theory can be extended to an excitation composed by a larger number of input signals.

The 3rd order PIM contributions are usually the dominating ones in practice, due to their higher power level and closeness to the RF transmission band [5], [24], [29]. Therefore, the classic polynomial model of a non-linear system with only 3rd order terms is considered from now on [10], [22]:

$$v_{\text{out}}(t) = C + \alpha v_{\text{in}}(t) + \gamma v_{\text{in}}^3(t) \tag{4}$$

Let us first consider the well-known case where the two input signals are CW tones:

$$v_{\text{in1}}(t) = A_1 \cos(2\pi f_1 t) \quad (4a)$$

$$v_{\text{in2}}(t) = A_2 \cos(2\pi f_2 t) \quad (4b)$$

assuming zero phase carriers, as it has been demonstrated that the phase of the carriers does not affect the PIM power level in a two-carrier PIM scenario [30].

By substituting (4a) and (4b) into (4), the ignited 3rd order PIM is composed of tones falling at frequencies f_1, f_2, $3f_1$, $3f_2$, $2f_1 \pm f_2$ and $2f_2 \pm f_1$ with different amplitude factors (AFs) as detailed in [17]–[19].

Let us focus on the term at $2f_2 - f_1$, which tends to be the most problematic one in many satellite payloads (as the uplink band is normally placed at slightly higher frequencies than the downlink band). The expression for this term is given by [19], [30]:

$$v_{\text{out}}(t) = \gamma \frac{3}{4} A_1 A_2^2 \cos(2\pi(2f_2 - f_1)t) \quad (5)$$

which corresponds to a Dirac's delta of amplitude $\gamma\frac{3}{4}A_1A_2^2$ at $2f_2 - f_1$ (and also at $-2f_2 + f_1$, as the spectrum of a real signal must be hermitian), being γ the coefficient of the third order term of the device non-linear model in (4), and $3/4$ the amplitude factor of this specific term [17].

This contribution comes from the term $3v_{\text{in1}}(t)v_{\text{in2}}^2(t)$ obtained after substituting (4a) and (4b) into (4). Let us derive a general expression for the spectrum of this term for arbitrary input stimulus. This can be accomplished by using the general Wiener-Volterra series analysis usually performed for AIM [19], [31], [32]. In this case, a more direct approach exploiting the Fourier transform is applied. Anyway, this is the first time a mathematical model is used to perform the spectral analysis of PIM under modulated signal excitation, thus allowing to predict and evaluate PIM interference for satellite communication systems.

Consider $F(f)$ and $G(f)$ as the Fourier transforms of the time-domain signals $f(t)$ and $g(t)$. The inverse Fourier transform of the convolution of $F(f)$ and $G(f)$ can be expressed as:

$$\begin{aligned}
&\mathscr{F}^{-1}\{(F * G)(f)\}(t) \\
&\quad = \int_{-\infty}^{\infty}\left(\int_{-\infty}^{\infty} F(\tau)\, G(f-\tau)\, d\tau\right) e^{\mathrm{j}2\pi f t} df \\
&\quad = \int_{-\infty}^{\infty} F(\tau)\left(\int_{-\infty}^{\infty} G(f-\tau)\, e^{\mathrm{j}2\pi f t} df\right) d\tau \quad (6)\\
&\quad = \int_{-\infty}^{\infty} F(\tau)\left(\int_{-\infty}^{\infty} G(u)\, e^{\mathrm{j}2\pi (u+\tau) t} du\right) d\tau \\
&\quad = \int_{-\infty}^{\infty} F(\tau)\, e^{\mathrm{j}2\pi\tau t} d\tau \int_{-\infty}^{\infty} G(u)\, e^{\mathrm{j}2\pi u t} du \\
&\quad = f(t)\cdot g(t) \quad (7)
\end{aligned}$$

so that the spectrum of the product of two time-domain signals is the convolution of the Fourier transform of both signals:

$$\mathscr{F}\{f(t)\cdot g(t)\} = F(f) * G(f) \quad (8)$$

This identity can be used to obtain a general expression for the spectrum of the term $3v_{\text{in1}}(t)v_{\text{in2}}^2(t)$ in the form:

$$\begin{aligned}
&\mathscr{F}\{3v_{\text{in1}}(t)v_{\text{in2}}^2(t)\}(f) = 3V_{\text{in1}}(f) * V_{\text{in2}}(f) * V_{\text{in2}}(f) \\
&\quad = \frac{3}{8}\left[\hat{X}(f - (2f_2 + f_1)) + \hat{X}^{\dagger}(f + (2f_2 + f_1))\right] \\
&\quad + \frac{3}{4}\left[\hat{X}(f - f_1) + \hat{X}^{\dagger}(f + f_1)\right] \\
&\quad + \frac{3}{8}\left[\hat{X}(f - (2f_2 - f_1)) + \hat{X}^{\dagger}(f + (2f_2 - f_1))\right] \quad (9)
\end{aligned}$$

where $\hat{X}(f)$ is given by:

$$\hat{X}(f) = \hat{V}_{\text{in1}}(f) * \hat{V}_{\text{in2}}(f) * \hat{V}_{\text{in2}}(f) \quad (10)$$

being $\hat{V}_{\text{in}k}(f)$ the spectrum of the equivalent baseband signal of $v_{\text{in}k}(t)$, which is obtained by performing a downwards shift f_k to the positive frequencies of $2V_{\text{in}k}(f)$ (i.e., $\hat{V}_{\text{in}k}(f) = 2u(f + f_k)\, V_{\text{in}k}(f + f_k)$, being $u(x)$ the unit step function) [33]. Note that for CW input stimulus of amplitude 1, $\hat{X}(f) = \delta(f)$, and expression (9) yields the known spectral terms coming from $3\cos(2\pi f_1 t)\cos^2(2\pi f_2 t)$.

From the different terms in (9), the one to be considered is $\frac{3}{8}\hat{X}(f - (2f_2 - f_1))$ (or its hermitian conjugate $\frac{3}{8}\hat{X}^{\dagger}(f + (2f_2 - f_1))$ in the negative frequency axis), as it represents the PIM term centered at $2f_2 - f_1$. It is worth pointing out that this term has the spectral shape of $\hat{X}(f)$ according to (10).

For the particular case of two CW input carriers, whose baseband equivalent signal is a Dirac's delta centered at the origin with the amplitude of the tone, the term $\hat{X}(f)$ is equal to $A_1A_2^2\delta(f)$, so that the last term in brackets in (9) can be expressed in the time domain as:

$$\frac{3}{4}A_1A_2^2\cos(2\pi(2f_2 - f_1)t) \quad (11)$$

which is the same expression in (5) once the coefficient γ of the non-linear model in (4) is incorporated.

The formulation derived in the above paragraphs allows to evaluate the PIM term associated to $2f_2 - f_1$ for two arbitrary input signals centered at f_1 and f_2, whose spectrum (which must be centered at $2f_2 - f_1$) can be expressed in general as:

$$A_{\text{PIM}}\hat{\hat{V}}_{\text{in1}}(f) * \hat{\hat{V}}_{\text{in2}}(f) * \hat{\hat{V}}_{\text{in2}}(f) \quad (12)$$

where $\hat{\hat{V}}_{\text{in}i}(f)$ is a normalized version of $\hat{V}_{\text{in}i}(f)$, so that the convolution of the three terms in (12) has a maximum value of unity.

In virtue of the theory detailed in Section II-A, the amplitude A_{PIM} is chosen to match the measured power level of the PIM term for the standard two-tone test with the same overall RF input power (in case the input power of both scenarios is not the same, the overall PIM output power for the modulated signal case can be estimated by using (1)). Note that according to [17], the PIM power must be distributed in the different third-order PIM terms. However, the amplitude factors for the same PIM term of the two-tone and modulated signal scenarios are identical, thus enabling a direct comparison between the PIM power levels of the contributions associated to $2f_2 - f_1$ for both types of signal excitation.

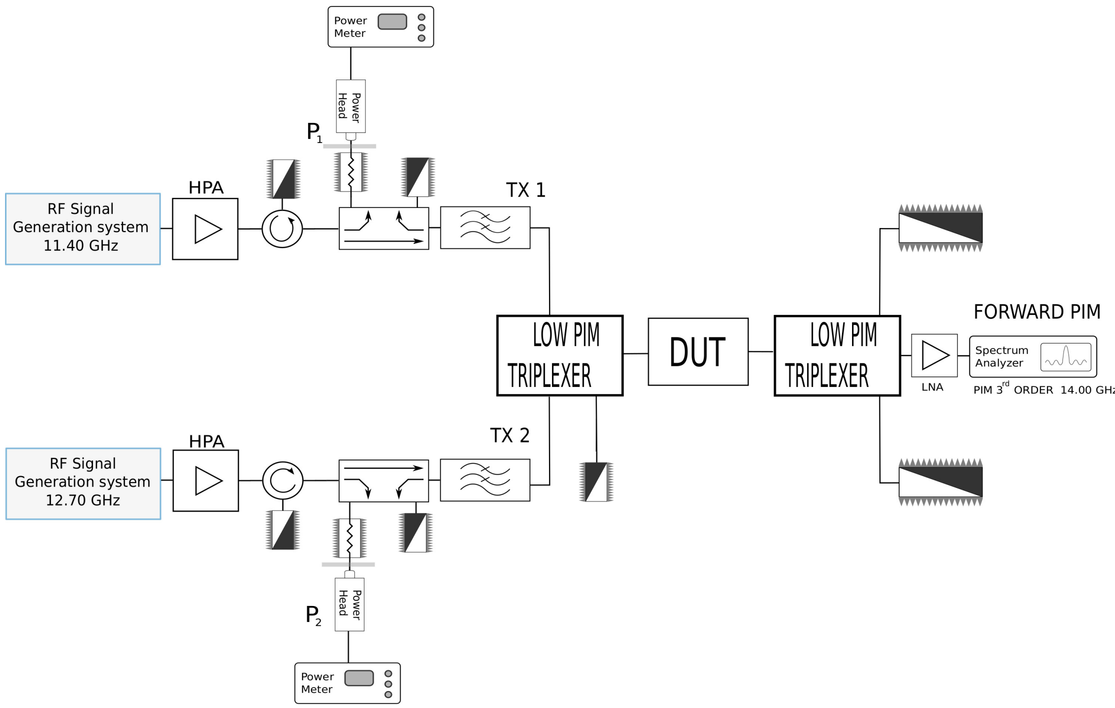

Fig. 2. Schematic of the PIM test set-up for conducting PIM measurements under modulated scenario.

The theory developed in this section can be extended, if required, to another PIM term of third order, or even of different order.

C. Approximate PIM Power Spectral Density

Consider two generic modulated signals centered at f_1 and f_2, with bandwidths B_1 and B_2, respectively, exciting a non-linear device with a joint RF input power level $IP\,(\text{dBm})$.

Let us suppose that a standard two-carrier test has been performed using CW signals at the frequencies f_1 and f_2 with the same overall input power, obtaining an output power OP_{PIM} for the PIM term of interest at $mf_1 \pm nf_2$ (being m and n positive integers). According to the PIM power conservation rule, the output power for such a PIM term originated in the modulated signal case should also be OP_{PIM} (in case the input power is different in both scenarios, the output power for the modulated signal excitation case can be estimated from (1)).

The convolution property in (8) implies that the bandwidth of the multiplication of two time domain signals is equal to the sum of the bandwidths of both signals [34]. As the PIM term associated to $mf_1 \pm nf_2$ is originated from $v_{\text{in}1}^m(t)v_{\text{in}2}^n(t)$, the bandwidth occupied by the PIM contribution is therefore:

$$B_{\text{PIM}} = mB_1 + nB_2 \tag{13}$$

If we assume that the power of this PIM term is uniformly distributed along its bandwidth, the PIM power spectral density can be expressed as:

$$OP_{\text{PIM}}\left(\frac{\text{dBm}}{\text{Hz}}\right) = OP_{\text{PIM}}\,(\text{dBm}) - 10\log_{10}\left(B_{\text{PIM}}\,(\text{Hz})\right) \tag{14}$$

Since the particular shape of the spectrum of the PIM contribution depends on the spectral distribution of the modulated signals and the specific PIM term of interest, the expression (14) must be considered as a first order approximation. However, it allows to establish a fast initial link between PIM specifications for CW and modulated input signals.

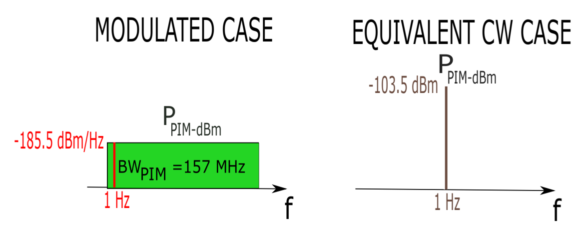

Fig. 3. Approximate method to link CW and modulated signal scenarios. For 157 MHz PIM bandwidth in the modulated case, the PIM level (in dBm measured in 1 Hz) is reduced in 82 dB with respect to the two-tone CW case.

For example, consider a PIM requisite of -185.5 dBm/Hz in a PIM bandwidth $B_{\text{PIM}} = 157$ MHz (see Fig. 3). This PIM spectral density corresponds, from (14), to an overall output power for the PIM term $OP_{\text{PIM}} = -103.5$ dBm. Therefore, in a classic two-tone CW test keeping the same power level for the two input channels, the measured PIM must be lower than -103.5 dBm. Note how the requirements for the CW and modulated cases differ severely. In fact, the direct transfer of a modulated PIM specification to a standard two-tone CW case would lead to overdemanding PIM requisites.

Since the PIM signal could have a non-uniform spectral distribution, a correction term must be added to (14) in order to relate, in a more accurate way, the PIM peak power level for modulated excitation with the CW case. In Section III, a rigorous analysis for the PIM term at $2f_2 - f_1$ originated from modulated signals with a rectangular-shaped spectrum, is carried out and experimentally verified.

(a) Front view

(b) Rear view

Fig. 4. Assembled set-up for performing PIM measurements under CW and modulated scenarios.

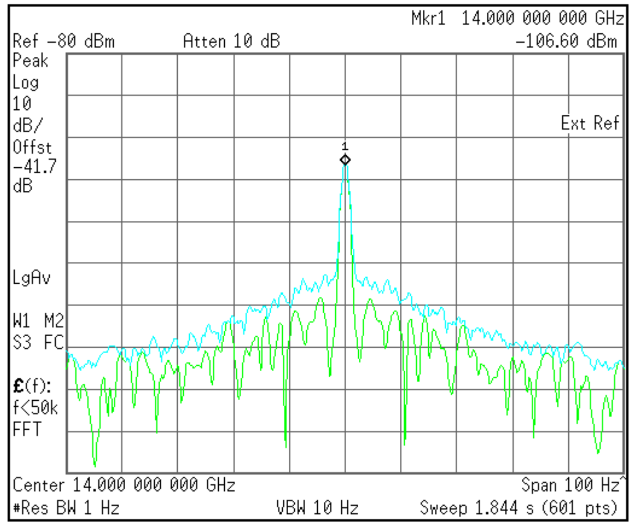

(a) CW-CW case

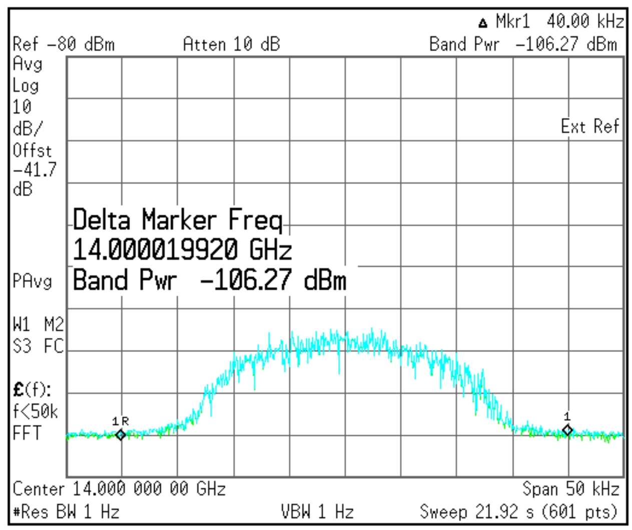

(b) 4QAM-4QAM case

Fig. 5. PIM power conservation. CW-CW case (top) versus 4QAM-4QAM brick-wall modulation with f_s=10 kbps (bottom).

III. Results

An extensive range of PIM measurements were carried out at Ku-band, in order to verify the theory described in Section II for PIM with modulated signals. Although this theory is partly based on well-established results for AIM, it is also combined with some PIM particularities. It is worth pointing out that any theoretical result for PIM requires an experimental validation, due to the intricacies of this subtle effect. To the authors' knowledge, this is the first time PIM measurements from a large test campaign involving modulated signals are reported.

The test campaign was carried out thanks to a dedicated PIM bench developed at the ESA-VSC European High Power RF Space Laboratory [35], able to combine two different signals (CW or modulated), and also evaluate the conducted 3$^{\text{rd}}$ order forward PIM corresponding to $2f_2 - f_1$. Fig. 2 depicts a scheme of the set-up. Some photos of the assembled test bed are shown in Fig. 4. Note that the bench uses a low-PIM triplexer at the input of the device under test (DUT) to combine two input channels (the third input channel is terminated in a matched load), whereas a low-PIM triplexer is placed at the output of the DUT to separate the high-power channels (each one absorbed by a separate dummy load) from the PIM signal. The weak PIM signal is delivered to a low-noise amplifier (LNA) before being detected with a spectrum analyzer.

The central frequencies of the input channels were chosen to be $f_1 = 11.4$ GHz and $f_2 = 12.7$ GHz, with an RF input power of 20 W per channel (both channels have the same power, according to the the IEC62037 standard [15]). The PIM signal at around f_{PIM}=14 GHz is measured, as corresponds to the $2f_2 - f_1$ PIM term.

Different modulations (QPSK, 8PSK, 4QAM and 16QAM) and symbol rates f_s (1 kbps, 5 kbps and 10 kbps) were considered during the tests. The pseudo-noise 9 (PN9) sequence of the Keysight E8267D signal generators were used to generate the modulated signals. A Root Rise Cosine (RRC) filter, with the roll-off factor α set to zero, was applied to emulate a brick-wall filter as best as possible. For this particular case, the spectrum of each modulated signal must have a shape similar to a rectangle with a bandwidth close to the symbol rate, leading to an ideal brick-wall modulation scheme.

A. Validation of the PIM Power Conservation Rule

The first set of experiments is conducted to accomplish two key objectives: analyse the effect of the different modulation schemes and symbol rates in the measured PIM signal spectrum, and also obtain a practical verification of the PIM power conservation rule proposed in [17] for modulated signal scenarios.

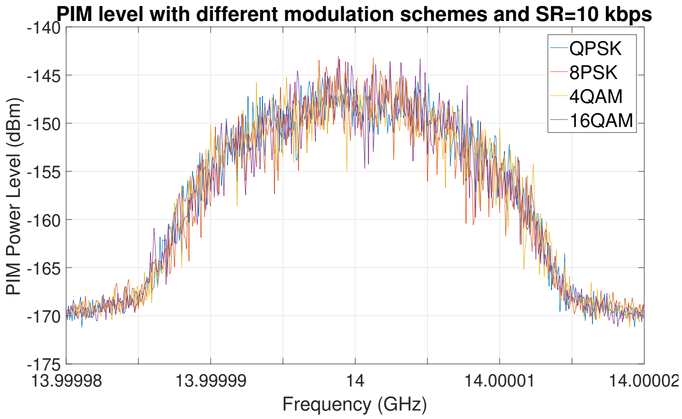

Fig. 6. Comparison of the measured spectrum of the $2f_2 - f_1$ PIM term for different modulation schemes sharing the same symbol rate of 10 kbps. All the modulated signals are, ideally, brick-wall (PN9 sequence with roll-off factor equal to zero).

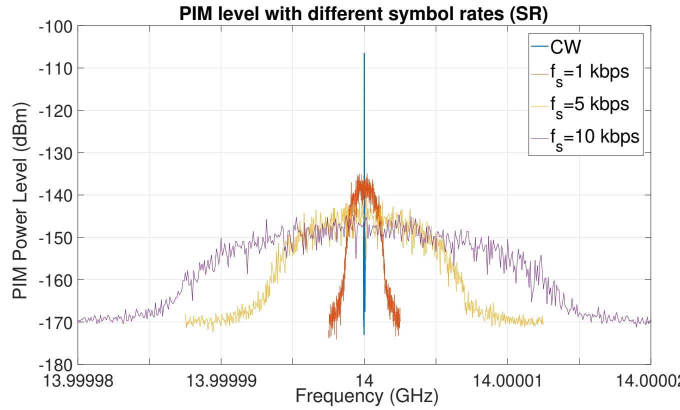

Fig. 7. Comparison of the measured spectrum of the $2f_2 - f_1$ PIM term for 4QAM brick-wall modulated signals with different symbol rate f_s. The reference CW-CW case (corresponding to a symbol rate of 0 kbps) is also plotted.

An initial reference test with CW carriers at f_1 and f_2 of 20 W of input power each is carried out (see Fig. 5a). Next, modulated signals of 20 W of input power are injected into each channel (see Fig. 5b). Both channels share the same modulation type and symbol rate f_s in all the experiments, using the PN9 pseudo-noise sequence as modulating signal. Since the input power at the DUT is the same for both the CW and modulated scenarios, the overall output PIM power corresponding to the $2f_2 - f_1$ term should also be the same, according to (1) and (2). This is illustrated in Fig. 5, where the PIM power in the CW case (measured at $f_{\text{PIM}} = 14$ GHz with a resolution bandwidth of 1 Hz) is -106.6 dBm, whereas for 4-QAM modulated signals with $f_s = 10$ kbps is -106.3 dBm (integrated along a 40 MHz bandwidth centered at $f_{\text{PIM}} = 14$ GHz). This represents a deviation of only 0.3 dB between the overall power predicted by the PIM power conservation rule (i.e., the value of -106.6 dBm measured in the CW case) and the PIM power measured when the DUT is excited with the modulated signals. Similar deviations between predicted and measured power levels, for the PIM term under study, were obtained for all the modulation schemes and symbol rates considered during the experiments. It is important to point out that the deviations observed are within the measurement error of the spectrum analyzer (+/-1 dB) and/or the typical fluctuation of PIM over time, thus they can be considered as negligible.

Fig. 6 shows the measured spectrum of the PIM signal corresponding to the $2f_2 - f_1$ term for QPSK, 8PSK, 4QAM and 16 QAM modulations with a symbol rate of 10 kbps. As it can be noticed, the spectrum of the PIM signal is roughly the same regardless the modulation scheme applied. These results support again the PIM power conservation rule, since the PIM power is maintained for the different modulation schemes, as long as the overall DUT input power is the same. From now onwards, only the 4QAM modulation is considered, as the modulation scheme does not have a relevant role in the spectrum of the measured PIM signal.

The effect of the symbol rate is analyzed next. Fig. 7 shows the spectrum of the PIM term associated to $2f_2 - f_1$ for 4QAM modulation with different symbol rates. As expected, the PIM signal is spread over the spectrum as the symbol rate increases. Note that the bandwidth of the modulated signals must be close to f_s since the signal generators use an RRC filter with a roll-off factor of zero. Therefore, a ten-fold increase in the symbol rate turns out into a 10 times larger PIM signal bandwidth. In addition, Fig. 7 also shows how the PIM power spectral density is reduced in about 10 dB in this case. As a result, the overall PIM power level is nearly the same regardless the symbol rate used.

This experimental study shows the real effect of the symbol rate and the modulated signal scheme in a PIM signal term. Besides, all the measured results provide more evidences to support the PIM power conservation rule enunciated in [17] for multicarrier scenarios, which has been extended in this work also to modulated signals. This principle is of the outmost relevance for this particular application, as it allows to determine the overall power level of a PIM term from a classic CW test, by just applying (1) and (2). In addition, in case the shape of the PIM signal spectrum is determined (using the tools presented in Section II-B), it allows to obtain the amplitude of the PIM signal. This point is validated experimentally in next Section III-B.

B. *PIM Signal Spectrum for Modulated Signals*

Following the theory developed in Section II-B, the equivalent baseband spectrum of the PIM term of interest associated to $2f_2 - f_1$ is given by (12). This expression involves convolutions of the spectrums $\hat{\tilde{V}}_{\text{in}k}(f)$ of the baseband equivalent representation of the input signals. As such spectrums are normalized so that the set of convolutions has a maximum value of 1, the spectral amplitude A_{PIM} can be expressed as:

$$A_{\text{PIM}} = \xi \sqrt{\frac{OP_{\text{PIM}}\,(\text{W})\,Z}{B_{\text{PIM}}}} \qquad (15)$$

and must be adjusted to match the overall power of the PIM term obtained from a standard CW test and the PIM power conservation rule (see Section II-A). The parameter Z

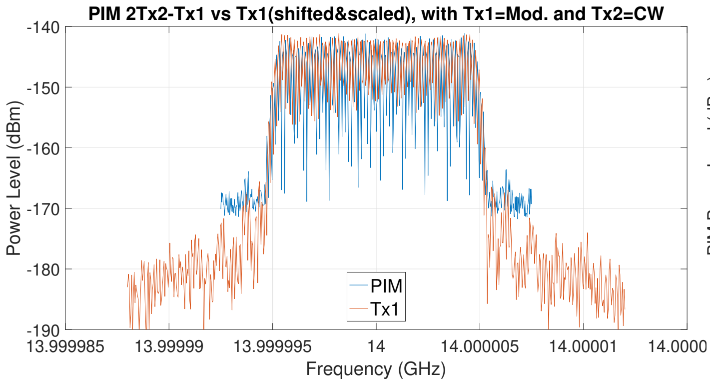

Fig. 8. Measurement comparison between $V_{\text{in}1}$ brick-wall modulated 4QAM signal with $f_s = 10$ kbps and $\alpha = 0$ (in brown), and 3^{rd} PIM order term at frequency $2f_2 - f_1$ (in blue). Note that $V_{\text{in}1}$ was shifted at the frequency $2f_2 - f_1$ and scaled in amplitude to enable a comparison with the PIM signal shape.

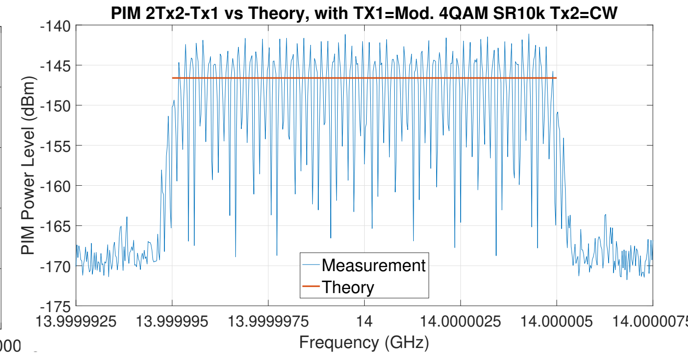

Fig. 9. 3^{rd} PIM contribution $2f_2 - f_1$ for the scenario where $V_{\text{in}1}$ is a 4QAM brick-wall modulated signal with $f_s = 10$ kbps and $\alpha = 0$, whereas $V_{\text{in}2}$ is a CW signal. The predicted PIM power spectral density in the passband is represented in red for comparison purposes.

represents the impedance level (required to relate power and voltage) of the RF port where the PIM signal is measured (typically, a spectrum analyzer), whereas ξ is a scaling parameter which takes into account the particular spectral distribution of the PIM term at $2f_2 - f_1$. In other words, ξ is a factor related to the spectral shape of the modulation considered for each case under analysis.

Let us consider three different cases depending on the type of signal (CW or modulated) used for each input. For the theoretical results, it is assumed an ideal brick-wall modulated signal with a flat spectrum along its bandwidth and zero outside, as corresponds to a noise signal filtered with an ideal Nyquist filter (i.e., an RRC filter with the roll-off factor α set to 0).

1) Signal 1 Modulated, Signal 2 CW: In this case, as the baseband spectrum of a CW signal is $A_{\text{CW}}\delta(f)$, the spectrum of the PIM term has the same shape of the modulated signal:

$$\begin{aligned} &\hat{\hat{V}}_{\text{in}1}(f) * \hat{\hat{V}}_{\text{in}2}(f) * \hat{\hat{V}}_{\text{in}2}(f) = \\ &\hat{\hat{V}}_{\text{in}1}(f) * \delta(f) * \delta(f) = \hat{\hat{V}}_{\text{in}1}(f) \end{aligned} \tag{16}$$

Therefore, the PIM signal must also have an ideal "brick" shape of width $B_{\text{PIM}} = B_1$. Once the spectrum of the PIM signal is determined, the parameter ξ can be derived. This is accomplished by equating the power associated to this spectrum to the output power OP_{PIM} of the PIM term, obtained after applying the PIM energy conservation rule (see (1) and (2)) to available measured data from the standard two-carrier (CW) PIM test. As the power in the baseband equivalent domain is twice the one in the passband domain, for this case it can be stated that:

$$\frac{A_{\text{PIM}}^2}{Z} B_{\text{PIM}} = 2OP_{\text{PIM}} \tag{17}$$

thus resulting in a value of $\xi = \sqrt{2}$ after comparing with (15). Note how the left term in (15) denotes the power of a spectrum of width B_{PIM} with uniform voltage amplitude A_{PIM}.

The experimental results for a 4QAM modulated signal with a symbol rate of 10 kbps and 20 W of input power at channel 1 are shown in Fig. 8. In addition to the measured PIM component corresponding to $2f_2 - f_1$, the plot also includes the spectrum of the input signal measured after replacing the channel 1 power meter (see Fig. 2) with an spectrum analyzer. To enable a comparison between both signals, the modulated signal has been shifted in frequency from 11.4 to 14 GHz, and also scaled in amplitude to match the power level of the PIM signal. According to the theoretical result (see (16)), the shape of the PIM signal is almost a replica of the shape of the modulated signal above the PIM noise floor of -170 dBm. It can be observed, however, how the E8267D signal generator provides a modulated signal with some spectral roll-off in spite of fixing α to zero, as an ideal brick-wall filter cannot be realized in practice. In any case, almost all of the power lies within the 10 kHz theoretical bandwidth.

Since the modulated signal has the same power of the CW signal of channel 1 used in Section III-A, the overall PIM power must be similar to the measured value of -106.6 dBm for the standard two-carrier case. This amount of power corresponds to a level of -146.6 dBm/Hz in a 10 kHz bandwidth. This predicted value has a difference of only 0.1 dB with the experimental mean PIM power level of -146.5 dBm in such frequency range, obtained from the spectrum analyzer measurements performed with a resolution bandwidth of 1 Hz (see Fig. 9). Again, this deviation can be considered negligible when compared to the measurement error of the spectrum analyzer and/or the fluctuation of PIM signal over time. Note that the PIM power in this case is uniformly distributed in the PIM bandwidth (13), resulting into the PIM power spectral density given by (14).

2) Signal 1 CW, Signal 2 Modulated: For the second scenario, a CW signal is used as channel 1 excitation, whereas the 4QAM modulated signal with a symbol rate of 10 kbps and a roll-off factor α set to zero is injected into channel 2. Both signals have a mean power level of 20 W. The shape of the equivalent baseband representation of the PIM signal should therefore be given by:

$$\begin{aligned} &\hat{V}_{\text{in}1}(f) * \hat{\hat{V}}_{\text{in}2}(f) * \hat{\hat{V}}_{\text{in}2}(f) = \\ &\quad \delta(f) * \hat{\hat{V}}_{\text{in}2}(f) * \hat{\hat{V}}_{\text{in}2}(f) = \hat{\hat{V}}_{\text{in}2}(f) * \hat{\hat{V}}_{\text{in}2}(f) \end{aligned} \tag{18}$$

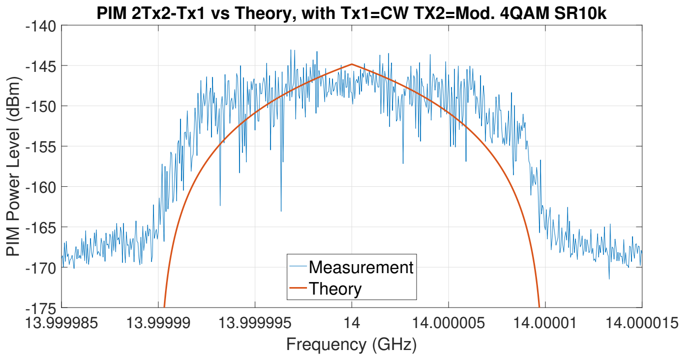

Fig. 10. Measured PIM signal at frequency $2f_2 - f_1$ for a 20 W CW signal at input channel 1 and a 20 W 4QAM brick-wall modulated signal with $f_s = 10$ kbps and $\alpha = 0$ at input channel 2, compared with the theoretical prediction.

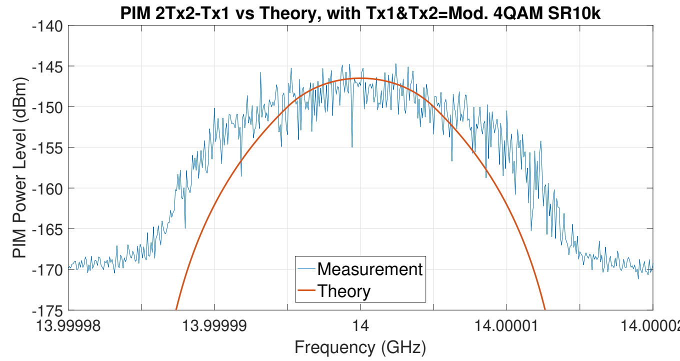

Fig. 11. Measured PIM signal at frequency $2f_2 - f_1$ for 20 W 4QAM brick-wall modulated signals with $f_s = 10$ kbps and $\alpha = 0$ for both input channels, compared with the theoretical prediction.

which corresponds to a triangular function with a normalized amplitude of 1 which extends from $-B_2$ to B_2, as $\hat{\hat{V}}_{\text{in}2}(f)$ has a rectangular shape of width B_2.

The expression that results after equating the PIM power of the equivalent baseband spectrum to the overall output power for the PIM contribution, OP_{PIM}, is now given by:

$$\frac{A_{\text{PIM}}^2}{3Z} B_{\text{PIM}} = 2OP_{\text{PIM}} \tag{19}$$

which differs from the one in (17) since the spectrum of the PIM signal has a triangular shape of width $B_{\text{PIM}} = 2B_2$ and amplitude A_{PIM} in this case. According to (15), this results in a value of $\sqrt{6} \simeq 2.45$ for the ξ parameter.

Let us now compare the PIM spectral peak power level for the two cases analyzed so far. This is equivalent to compare A_{PIM}, as $\hat{\hat{V}}_{\text{in}i}(f)$ are normalized so that the maximum value of the joint convolution in (12) is set to 1. Since the overall input PIM power and impedance level are the same for both cases, from (15) follows:

$$\frac{A_{\text{PIM,II}}}{A_{\text{PIM,I}}} = \frac{\xi_{\text{II}}}{\xi_{\text{I}}} \sqrt{\frac{B_{\text{PIM,I}}}{B_{\text{PIM,II}}}} = \frac{\sqrt{6}}{\sqrt{2}} \sqrt{\frac{B_1}{2B_2}} = \sqrt{\frac{6B_1}{4B_2}} \tag{20}$$

where the subindexes I and II denote the cases 1) (signal 1 modulated, signal 2 CW) and 2) (signal 1 CW, signal 2 modulated), respectively. Assuming that the bandwidth of the modulated signal is the same in both scenarios, so that $B_1 = B_2$, the PIM spectral peak power in case 2) is

$$20 \log_{10} \left(\frac{\sqrt{6}}{2} \right) = 1.76 \text{ dB} \tag{21}$$

higher than the one for case 1) in theory.

The comparison between the theoretical prediction and the measured PIM spectrum for the term corresponding to $2f_2 - f_1$ is shown in Fig. 10. Note how the predicted PIM peak power level is 1.76 dB higher than in Fig 9. As it can be observed, also in this case the model is able to provide a good match with the measurements in terms of both PIM level and spectral distribution. The slight deviation between the model and the measurement at the band edges can be attributed again to the non-ideal (i.e., non brick-wall) behaviour of the signal generator E8267D used for $V_{\text{in}2}$.

3) Signal 1 Modulated, Signal 2 Modulated: In the last scenario under consideration, two 4QAM brick-wall modulated signals with 10 kbps of symbol rate (and roll-off factor $\alpha = 0$) were used as excitation signals for the input channels (each using a different pseudo-noise PN9 modulating signal). In this case, the equivalent baseband spectrum has the general form given by (12). Assuming that the two modulated input signals have a rectangular shape with the same bandwidth $B_1 = B_2 = B$ (similar case to the usual one in satellite communications), the voltage spectrum of the equivalent baseband signal can be expressed as:

$$\hat{V}_{\text{PIM}}(f) = \begin{cases} \frac{2}{3} A_{\text{PIM}} \left(\frac{3}{2} + \frac{f}{B} \right)^2 & , -\frac{3}{2} \leq \frac{f}{B} \leq -\frac{1}{2} \\ A_{\text{PIM}} \left(1 - \frac{4}{3} \left(\frac{f}{B} \right)^2 \right) & , -\frac{1}{2} \leq \frac{f}{B} \leq \frac{1}{2} \\ \frac{2}{3} A_{\text{PIM}} \left(\frac{3}{2} - \frac{f}{B} \right)^2 & , \frac{1}{2} \leq \frac{f}{B} \leq \frac{3}{2} \\ 0 & \text{otherwise} \end{cases} \tag{22}$$

Following the same procedure for the two previous cases, which involves integrating the square of (22), we obtain:

$$\frac{44 A_{\text{PIM}}^2}{135Z} B_{\text{PIM}} = 2OP_{\text{PIM}} \tag{23}$$

where B_{PIM} is now given by $2B_2 + B_1 = 3B$ in virtue of (13). The parameter ξ takes therefore the value $\sqrt{135/22} \simeq 2.477$ after substituting (23) in (15). In a similar way to (20) and (21), we can obtain the variation in the PIM spectral peak power level with respect to case 1) by just comparing A_{PIM}, which results in an increase of only

$$20 \log_{10} \left(\sqrt{\frac{135/22}{2} \cdot \frac{1}{3}} \right) = 0.10 \text{ dB} \tag{24}$$

as the differences in the ξ parameter and in the PIM bandwidth B_{PIM} with respect to the case 1 (signal 1 modulated, signal 2 CW) nearly cancel out. A predicted PIM peak power level of -146.5 dBm is thus obtained for case 3), since the theoretical PIM power level for case 1) is -146.6 dBm.

This effect can be observed in Fig. 11, where the peak of the measured PIM power spectral distribution (taking the average value of the measured PIM oscillations) is about -146.5 dBm for a resolution bandwidth of 1 Hz. The shape of the measured spectrum for the 3rd order PIM contribution associated to the $2f_2 - f_1$ term, for the case of using the 4QAM modulating signals as inputs, is also very close to the theoretical predictions. Note that the enlargement in the measured PIM spectrum width with respect to the predicted one is caused by the non-ideal skirts of the RRC filter with $\alpha = 0$ implemented by the signal generators. In any case, an excellent agreement between measurements and predictions is also obtained for this case, which is the closest one to the most usual real scenario in satellite communications.

Note that the simplistic model presented in Section II-C can also be used to estimate the PIM power spectral density in modulated signal scenarios. This model assumes a uniform spectral distribution, which corresponds to the case 1 (signal 1 modulated, signal 2 CW). However, for the other two cases under analysis, this approach tends to underestimate the peak PIM power level. This can be corrected by taking into account the difference in the ξ parameter in (15). For this last case, involving modulated signals with rectangular-shaped spectrum at each input channel, the PIM power spectral density obtained from (14)

$$\begin{aligned} OP_{\text{PIM}} &= -106.6 \text{ dBm} - 10\log_{10}(30 \text{ kHz}) \\ &= -151.37 \ \frac{\text{dBm}}{\text{Hz}} \end{aligned} \tag{25}$$

must be increased in

$$20\log_{10}\left(\frac{\xi_{\text{III}}}{\xi_{\text{I}}}\right) = 20\log_{10}\left(\frac{2.477}{\sqrt{2}}\right) = 4.87 \text{ dB} \tag{26}$$

to obtain a more accurate prediction for the peak PIM power spectral density, resulting in the same theoretical value of -146.5 dBm previously obtained for this last third case. Note how expressions (25) and (26) provides a more direct way of evaluating the peak PIM power level. This process can also be useful for transferring, in a more rigorous way, CW and modulated signal PIM specifications.

IV. Conclusion

This paper presents a novel techinque able to determine the PIM power spectral density for modulated signal scenarios, based on measured results from the standard (and simpler) IEC62037 test with two CW input signals. The method successfully combines an spectral approach with a PIM power conservation rule recently postulated.

Measured PIM data obtained from a non-linear device excited with modulated signals are reported. Although the theory can be extended for an arbitrary PIM term, the paper focuses on the most problematic one in satellite communication, corresponding to the $2f_2 - f_1$ PIM contribution. Several cases are analyzed in an extensive test campaign (considering different modulations, symbol rates and combinations of CW and modulated input signals with rectangular-like shaped spectrum), providing very valuable experimental results.

An excellent agreement between the predictions and the measured results has been obtained in all cases, fully validating the theoretical model proposed. In addition, the power conservation rule has also been experimentally verified for modulated signals. This implies a distribution of the PIM signal over a bandwidth proportional to the order of the PIM term. This spreading of the PIM energy results in a severe reduction of the peak PIM power level with respect to the CW case. The latter is of paramount importance for the PIM qualification of space devices, because a classic PIM CW test might provide in most of the cases a severe over-testing of the unit, especially when input channels with wide bandwidths are involved.

The technique described in this paper, allows to estimate the peak PIM power spectral density for a modulated signal scenario from standard CW tests. In addition, it also enables the transformation of PIM specifications/data from CW to modulated signal excitations, or vice-versa, using simple expressions.

Acknowledgment

The authors would like to acknowledge the ESA-VSC European High Power RF Space Laboratory for its contribution to this work - A laboratory funded by the European Regional Development Fund - A way of making Europe.

References

[1] J. G. Dumoulin, "Passive intermodulation and its effect on space programs," in *Proc. IEE Colloquium on Screening Effectiveness Measurements (Ref. No. 1998/452)*, London, UK, May 1998, pp. 3/1–3/34.

[2] C. Hoeber, D. Pollard, and R. Nicholas, "Passive intermodulation product generation in high power communications satellites," in *Proc. 11th AIAA Int. Comm. Satellite Syst. Conf.*, San Diego, CA, Mar. 1986, pp. 361–365.

[3] F. Carducci, "Passive intermodulations aspects on ITALSAT F2/EMS spacecraft," in *Proc. of Int. Symp. on Antenna Technology and Applied Electromagnetics*, Ottawa, ON, Canada, Aug. 1994, pp. 377–380.

[4] J. W. Boyhan and H. F. Lenzing, "Satellite passive intermodulation: system considerations," *IEEE Trans. Aerosp. Electron. Syst*, vol. 32, no. 3, pp. 1058–1064, July 1996.

[5] R. J. Cameron, C. M. Kudsia, and R. R. Mansour, *Microwave Filters for Communication Systems: Fundamentals, Design and Applications*, 2nd ed. Hoboken, NJ, USA: John Wiley & Sons, 2018.

[6] R. Piazza, B. Shankar, M. R. Rao, and B. Ottersen, "Data predistortion for multicarrier satellite using orthogonal memory polynomials," in *Proc. 14th IEEE Workshop Signal Process. Adv. Wirel. Commun.*, Darmstadt, Germany, Sep. 2007, pp. 689–693.

[7] H. Zhang, Y. Zhang, C. Huang, Y. Yuan, and L. Cheng, *Spacecraft Electromagnetic Compatibility Technologies*. Singapore: Springer, 2020.

[8] J. Christensen, "ITU regulations for Ka-band satellite networks," in *Proc. 30th AIAA Int. Comm. Satellite Syst. Conf.*, Ottawa, ON, Canada, Sep. 2012, pp. 524–527.

[9] H. Fenech, S. Amos, S. Tomatis, and V. Soumpholphakdy, "High throughput satellite systems: an analytical approach," *IEEE Trans. Aerosp. Electron. Syst.*, vol. 51, no. 1, pp. 192–202, Jan. 2015.

[10] R. Kwiatkowski, M. Vladimirescu, and K. Engel, "Tunnel conduction consequences in high frequency microcontacts; passive intermodulation effect," in *Proc. 50th IEEE Holm Conf. on Electrical Contacts*, Seattle, WA, USA, Sep. 2004, pp. 152–159.

[11] J. Russer, A. Ramachandran, A. Cangellaris, and P. Russer, "Phenomenological modeling of passive intermodulation (PIM) due to electron tunneling at metallic contacts," in *2006 IEEE MTT-S Int. Microw. Symp.*, San Francisco, CA, USA, Jun. 2006, pp. 1129–1132.

[12] J. Wilkerson, K. Gard, A. Schuchinsky, and M. Steer, "Electro-thermal theory of intermodulation distortion in lossy microwave components," *IEEE Trans. Microw. Theory Techn.*, vol. 56, no. 12, pp. 2717–2725, Dec. 2008.

[13] S. Zhang, X. Zhao, F. Gao, and Y. He, "Study of metal contact resistance and its statistical correlationship with passive intermodulation," in *Proc. IEEE Annu. Holm Conf. Electr. Contacts*, Albuquerque, NM, USA, Oct. 2018, pp. 1–6.

[14] P. Lui, "Passive intermodulation interference in communication systems," *Electronics and Communication Engineering Journal*, vol. 2, no. 3, pp. 109–118, June 1990.

[15] *Passive RF and Microwave Devices, Intermodulation Level Measurement*, International Electrotechnical Commission (IEC) Std. IEC62 037-1 to -6, 2012–2013.

[16] H. Hausman, *Fundamentals of satellite communications, part III*. USA: MITEQ Inc., 2009.

[17] D. Smacchia, P. Soto, V. E. Boria, and D. Raboso, "A new model to determine passive intermodulation terms when non-contributing carriers are added to classical scenarios," *IEEE Access*, vol. 9, pp. 152 070 – 152 074, Nov. 2021.

[18] J. Bussgang, L. Ehrman, and J. W. Graham, "Analysis of nonlinear systems with multiple inputs," *Proceedings of the IEEE*, vol. 62, pp. 1088 – 1119, Aug. 1974.

[19] D. Weiner and J. Spina, *Sinusoidal analysis and modeling of weakly nonlinear circuits*. New York, NY, USA: Van Nostrand Reinhold, 1980.

[20] M. Alizadeh and D. Rönnow, "A two-tone test for characterizing nonlinear dynamic effects of radio frequency amplifiers in different amplitude regions," *Measurement*, vol. 89, pp. 273–279, Jul. 2016.

[21] C. Kudsia, K. Ainsworth, J. Heierli, and F. Daniels, "A high power low passive intermodulation (PIM) UHF duplexer for space application," in *1979 IEEE MTT-S Int. Microw. Symp. Digest*, 1979, pp. 437–439.

[22] J. Henrie, A. Christianson, and W. Chappel, "Linear-nonlinear interaction's effect on the power dependence of nonlinear distortion products," *Applied Physics Letters*, vol. 94, no. 11, pp. 114 101–1–3, March 2009.

[23] S. Shayegani, J. Salmon, and R. Singh, "Multicarrier PIM behavior and testing in communications satellites," in *9th Int. Workshop on Multipactor, Corona and Passive Intermodulation (MULCOPIM)*, ESA/ESTEC, Noordwijk, The Netherlands, Apr. 2017, pp. 1–11.

[24] M. Silicani and S. Ricard, "Presentation of MDA PIM test facility capabilities and studies of PIM order amplitude relationship and PIM level variation as a function of transmit power flux density," in *9th Int. Workshop on Multipactor, Corona and Passive Intermodulation (MULCOPIM)*, ESA/ESTEC, Noordwijk, The Netherlands, Apr. 2017, pp. 1–9.

[25] B. Rosenberger, "The measurement of intermodulation products on passive components and transmission lines," in *50th ARFTG Conference Digest*, Portland, OR, USA, Dec. 1997, pp. 13–22.

[26] B. Deats and R. Hartman, "Measuring the passive-IM performance of RF cable assemblies," *Microw. RF Eng.*, vol. 36, pp. 108–114, Mar. 1997.

[27] D. S. Kozlov, A. P. Shitvov, A. G. Schuchinsky, and M. B. Steer, "Passive intermodulation of analog and digital signals on transmission lines with distributed nonlinearities: Modelling and characterization," *IEEE Trans. Microw. Theory Techn.*, vol. 64, no. 5, pp. 1383–1395, May 2016.

[28] J. Luo, L. Bi, C. Wang, D. Han, and T. Li, "A study of passive intermodulation of analog modulated signals in coaxial connectors," in *4th Int. Conf. Advanced Electronic Materials, Computers and Software Engineering (AEMCSE)*, Changsha, China, Mar. 2021, pp. 905–908.

[29] Q. Jin, J. Gao, G. T. Flowers, Y. Wu, and G. Xie, "Modeling of passive intermodulation with electrical contacts in coaxial connectors," *IEEE Trans. Microw. Theory Techn.*, vol. 66, no. 9, pp. 4007–4016, Sep. 2018.

[30] D. Smacchia, P. Soto, V. E. Boria, O. Monerris, J. Ossorio, D. Raboso, J. V. Morro, and M. Martínez-Mendoza, "Practical characterization of the effect of the transmission carrier phases in passive intermodulation," *IEEE Trans. Microw. Theory Techn.*, Apr. 2024, early access.

[31] N. Wiener, "Response of a non-linear device to noise," MIT. Radiation Lab., Cambridge, MA, USA, Tech. Rep. R-129, Apr. 1942.

[32] V. Volterra, *Theory of Functionals and of Integral and Integro-Differential Equations*. New York, NY, USA: Dover Publications, 1959.

[33] J. G. Proakis, *Digital Communications*, 4th ed. New York, NY, USA: McGraw-Hill, 2000.

[34] R. Baraniuk, *Signals and Systems*. Gainesville, FL, USA: University Press of Florida, 2009.

[35] ESA-VSC European High-Power RF Space Laboratory. European Space Agency and Val Space Consortium. Valencia, Spain. [Online]. Available: http://www.val-space.com/